Research Article
doi.org/10.1002/slct.202504450

Chemistry Europe
European Chemical Societies Publishing

www.chemistryselect.org

Boosting Efficient Nitrate Electrosynthesis by Pb/PdO-TiO2@2-MeIm/PPy/GO

Hui Mao,[a] Yuheng Sun,[a] Huinan Li,[a] Daliang Liu,[a] Qiong Wu,[a] Shuyao Wu,*[a] and Rui Zhang*[b, c]

Nitrate is vital in agriculture and industry, but the traditional Ostwald process for nitric acid production is energy-intensive and environmentally harmful. As a more sustainable alternative, the electrocatalytic nitrogen oxidation reaction (NOR) converts N_2 into nitrate under mild conditions using specific catalysts. Recent advancements have demonstrated that Pd and TiO_2 nanoparticles anchored on 2-methylimidazolium functionalized polypyrrole/graphene oxide (2-MeIm/PPy/GO) exhibit NOR activity. However, limited loading capacity under room temperature conditions hampers performance. This study improves catalytic efficiency using a hydrothermal method, achieving a maximum nitrate yield of 34.14 μg h^{-1} $mg^{-1}_{act.}$ at 2.04 V (versus reversible hydrogen electrode). and a Faraday efficiency of 5.28%. Characterization reveals that Pd sites facilitate N_2 conversion, while TiO_2 supports the necessary oxygen evolution reaction (OER) activity.

1. Introduction

Nitrate plays a crucial role in various sectors, including agriculture and industry, and is widely employed in the manufacture of fertilizers, explosives, pharmaceuticals, dyes, and emulsifiers.[1] The traditional Ostwald process for nitric acid production indeed comes with several challenges, including high energy consumption and environmental pollution.[2] The process involves the oxidation of ammonia to produce nitric acid, which requires high temperatures and pressures, leading to substantial energy usage and greenhouse gas emissions. Therefore, seeking environmentally friendly and low-consumption synthesis methods for nitrate production has been one of the focal points of the industrial and research fields. Electrocatalytic nitrogen oxidation reaction (NOR) can convert N_2 into nitrate with high efficiency and excellent selectivity in mild reaction conditions by some specific catalysts, which is indeed a promising alternative method for nitrate production.[3] The development of efficient NOR electrocatalysts is particularly important, which will provide feasibility for the green synthesis of nitrate. However, most reports are focused on exploring the electrocatalysts for the electrosynthesis of ammonia,[4–8] and there are relatively few reports on the electrosynthesis of nitrate.

NOR involves a 10-electron oxygen-coupled process and typically competes with the 4-electron oxygen evolution reaction (OER).[9] Enhancing the yield of nitrate nitrogen necessitates inhibiting OER while promoting the conversion of N_2 to NO* intermediates. However, a non-electrochemical step within the NOR process is critically constrained by the OER activity, on which the generation of O* for nitrate production depends.[10] Consequently, the design and synthesis of efficient NOR electrocatalysts encounter significant hurdles. Previous studies have shown that various materials, such as noble metals,[11] atomically dispersed metal-based catalysts[12] and spinel oxides,[13] exhibit some NOR electroactivity. Nonetheless, the inert nature of N_2 molecules and the competition from OER continue to impede the development of highly efficient NOR catalysts.

Recently, at room temperature, Pd and TiO_2 nanoparticles were anchored onto 2-methylimidazolium functionalized polypyrrole/graphene oxide (2-MeIm/PPy/GO), resulting in a composite with specific electrocatalytic performance for NOR.[14] However, due to the limited loading capacity of Pd and Ti caused by the simple reaction conditions at room temperature, the electrocatalytic NOR activity of the composite is suboptimal and unsatisfactory. Herein, a hydrothermal method was used to enhance the loading capacity of Pd and Ti, thereby optimizing the obtained Pb/PdO-TiO_2@2-MeIm/PPy/GO for electrocatalytic NOR. A maximum NO_3^- yield of 34.14 g h^{-1} $mg^{-1}_{act.}$ at 2.04 V (versus reversible hydrogen electrode (RHE)) was recorded, alongside a corresponding Faraday efficiency (FE) of 5.28%, detected by ion chromatography (IC) and calculated by a standard curve (Figure S1). By comparing the characterization results of Pb/PdO-TiO_2@2-MeIm/PPy/GO before and after NOR treatment, the conversions of the inert N_2 to active *NO intermediates mostly took place at Pd-site in Pd/PdO-TiO_2@2-MeIm/PPy/GO, while TiO_2 provided

[a] H. Mao, Y. Sun, H. Li, D. Liu, Q. Wu, S. Wu
Institute of Clean Energy Chemistry, Key Laboratory for Green Synthesis and Preparative Chemistry of Advanced Materials, College of Chemistry, Liaoning University, Shenyang 110036, P.R. China
E-mail: sywu@lnu.edu.cn

[b] R. Zhang
Shenyang Key Laboratory of Medical Molecular Theranostic Probes in School of Pharmacy, School of Pharmacy, Shenyang Medical College, Shenyang 110034, P.R. China
E-mail: ruizhang@symc.edu.cn

[c] R. Zhang
College of Pharmaceutical Engineering, Shen Yang Pharmaceutical University, Shenyang 110016, P.R. China

Supporting information for this article is available on the WWW under https://doi.org/10.1002/slct.202504450

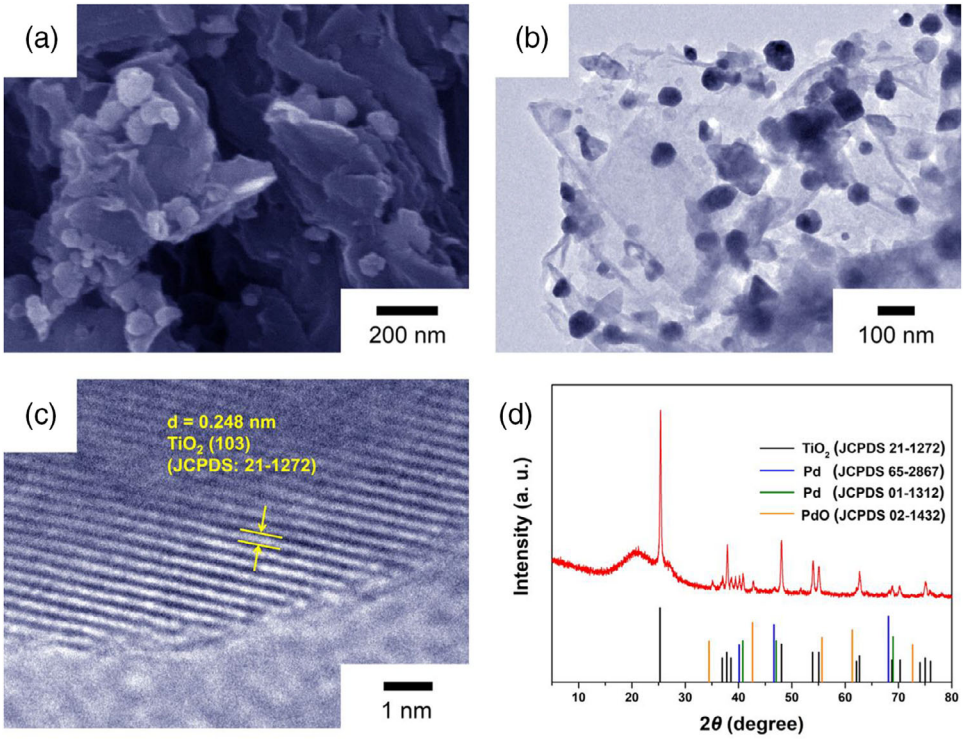

Figure 1. (a) SEM, b) TEM, c) HRTEM image (SAED pattern, inset), and d) XRD pattern of Pd/PdO-TiO_2@2-MeIm/PPy/GO.

the appropriate OER activity for generating *O and further accelerating the non-electrochemical step of NOR.

2. Results and Discussion

The morphology of Pd/PdO-TiO_2@2-MeIm/PPy/GO, synthesized using the hydrothermal method, is depicted in Figure 1a,b. It displays a characteristic layered nanostructure with numerous distinct nanoparticles randomly distributed on certain curled sheet surfaces. The high-resolution transmission electron microscopy (HRTEM) image of the Pd/PdO-TiO_2@2-MeIm/PPy/GO (Figure 1c) reveals a distinct lattice plane is visible, with the lattice spacing calculated as 0.248 nm, corresponding well to the (103) crystallographic plane of the anatase TiO_2 (JCPDS file No. 21-1272). In addition to identifying the characteristic peaks of anatase TiO_2, the X-ray diffraction (XRD) pattern of the Pd/PdO-TiO_2@2-MeIm/PPy/GO in Figure 1d also reveals the characteristic peaks of Pd and PdO, consistent with Pd (JCPDS file No. 65-2867 and 01-1312), as well as PdO (JCPDS file No. 02-1432), which well indicate the coexistence of Pd/PdO and TiO_2 in the synthesized material.

The electrocatalytic performance of Pd/PdO-TiO_2@2-MeIm/PPy/GO for NOR is systematically investigated in an H-type cell employing 0.1 M KOH electrolyte using various electrochemical techniques. The NOR process on Pd/PdO-TiO_2@2-MeIm/PPy/GO modified carbon cloth (CC) in 0.1 M KOH solution containing saturated N_2 is illustrated in Scheme 1. Polarization curves of Pd/PdO-TiO_2@2-MeIm/PPy/GO are presented in Figure 2a, obtained through linear sweep voltammetry (LSV) under N_2 and Ar-saturated electrolytes. Notably, at potentials

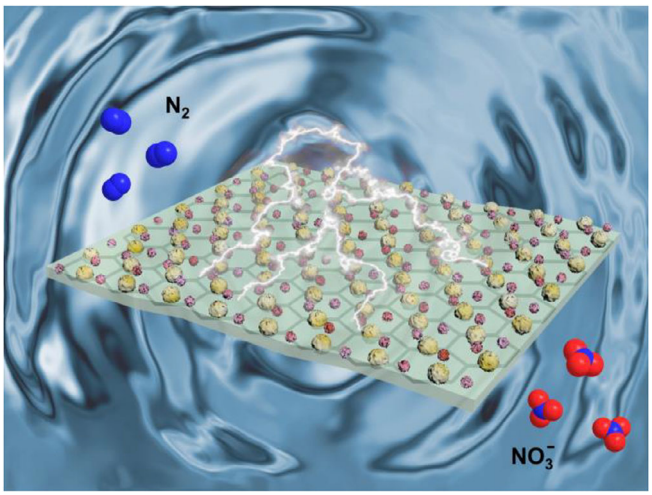

Scheme 1. The NOR process on Pd/PdO-TiO_2@2-MeIm/PPy/GO modified CC in 0.1 M KOH solution containing saturated N_2.

between 1.8 and 2.5 V (versus RHE), the current density (j) under N_2-saturated conditions is higher than that in the Ar-saturated electrolyte, suggesting that NOR can be effectively catalyzed by Pd/PdO-TiO_2@2-MeIm/PPy/GO. The NO_3^- yield and FE derived from chronoamperometry (CA) tests serve as critical metrics for assessing the performance of NOR electrocatalysts. Obviously depicted in Figure 2b, the highest NO_3^- yield of 34.14 μg h^{-1} mg^{-1}_{act}, is observed at 2.04 V (versus RHE), with a corresponding FE of 5.28%. Though 1.84 V (versus RHE) provides the highest FE, the NO_3^- yield was much lower than that obtained at 2.04 V, indicating that a slightly higher potential like 2.04 V

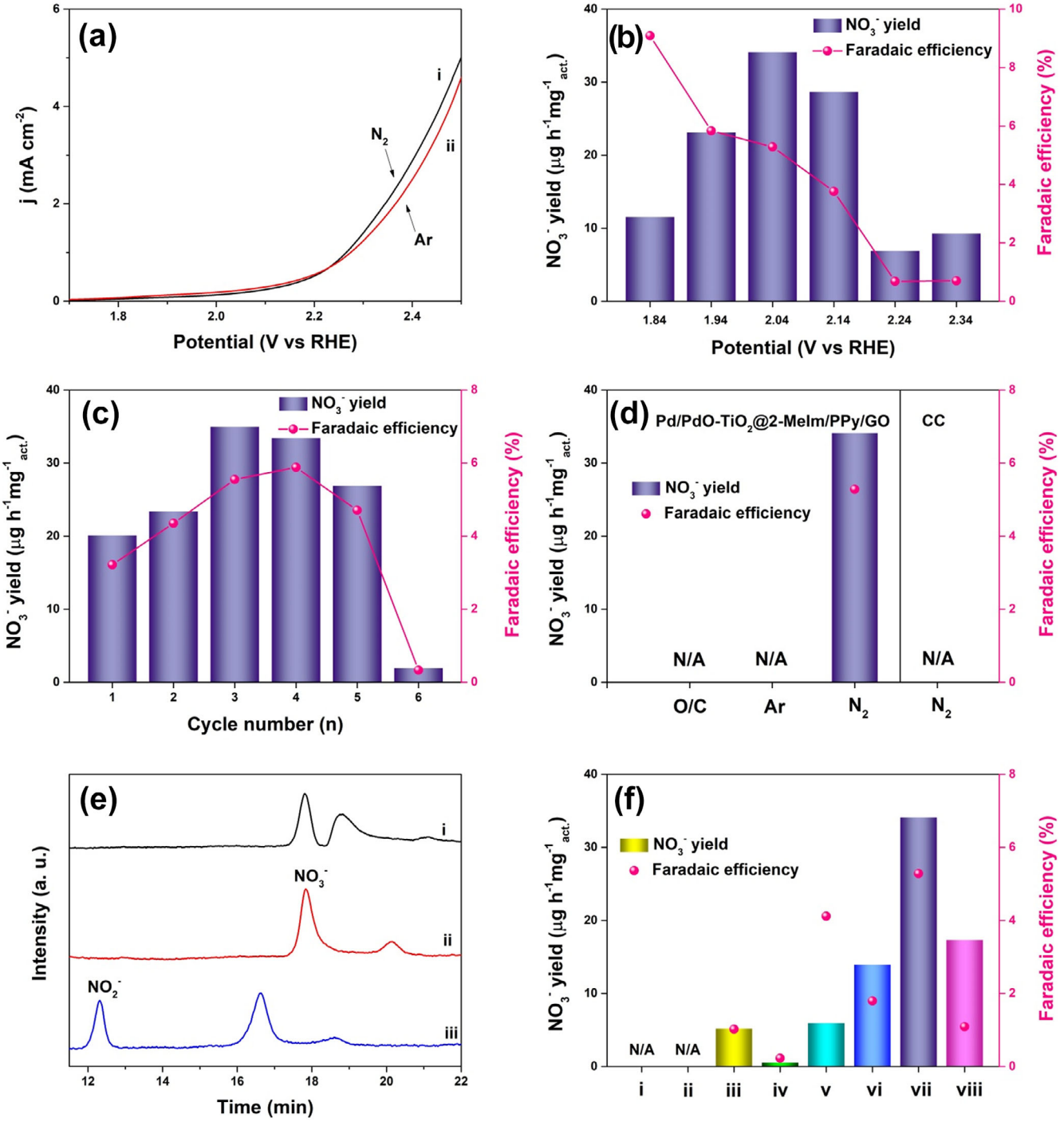

Figure 2. a) Linear sweep voltammograms of Pd/PdO-TiO_2@2-MeIm/PPy/GO under saturated Ar and N_2 in 0.1 M KOH; b) the NO_3^- yield and FE of Pd/PdO-TiO_2@2-MeIm/PPy/GO for NOR at different potentials (versus RHE); c) recycling test for Pd/PdO-TiO_2@2-MeIm/PPy/GO at 2.04 V under electrolysis for 2 h performed six times; d) the electroactivity of CC (substrate) and Pd/PdO-TiO_2@2-MeIm/PPy/GO toward NOR at 2.04 V under different conditions; e) ion chromatogram spectra of (i) electrolyte after NOR by Pd/PdO-TiO_2@2-MeIm/PPy/GO at 2.04 V, (ii) the standard NO_3^- of 0.2 mg mL^{-1}, (iii) the standard NO_2^- of 0.2 mg mL^{-1}; f) the NO_3^- yield and FE obtained by different electrocatalysts at 2.04 V under electrolysis for 2 h: (ai) GO, (ii) PPy/GO, (iii) 2-MeIm/PPy/GO, iv) Pd/PdO-TiO_2, (v) Pd/PdO-TiO_2@GO, (vi) Pd/PdO-TiO_2@PPy/GO, (vii) Pd/PdO-TiO_2@2-MeIm/PPy/GO and (viii) TiO_2@2-MeIm/PPy/GO.

might enhance the reaction kinetics further. In addition, the current density was extremely low at potentials before 1.84 V, resulting in the poor NOR process. The FE of Pd/PdO-TiO_2@2-MeIm/PPy/GO at potentials before 1.84 V was lower than 2%, because the reaction kinetics may not be as favorable. The catalyst may not be fully activated at these lower voltages, leading to a lower NOR rate. The stability of the electrocatalyst is another crucial aspect for NOR performance. The NO_3^- yield and FE of Pd/PdO-TiO_2@2-MeIm/PPy/GO after 6 cycles at 2.04 V (versus RHE) are presented in Figure 2c. Following 5 cycles, there is no notable reduction in NO_3^- yield and corresponding FE, maintaining values of 26.92 μg h^{-1} $mg^{-1}_{act.}$ and 4.71%. However,

a significant drop in NO_3^- yield and FE is observed after the 6th cycle, possibly attributed to the extended NOR reaction leading to a loss in NOR activity of the material. In order to delve deeper into the nitrogen source contributing to the produced NO_3^-, potential interferences from the electrolyte, electrocatalyst, and raw gas are meticulously eliminated, with a 2-h NOR test conducted under distinct conditions: N_2-saturated electrolyte in the absence of an external potential (O/C), Ar-saturated electrolyte at 2.04 V, and using a CC substrate. Figure 2d reveals that only NO_3^- is produced when using Pd/PdO-TiO_2@2-MeIm/PPy/GO as the catalyst in N_2-saturated electrolyte at 2.04 V (versus RHE), while no NO_3^- is observed under the other conditions, suggesting that all the detected NO_3^- are originated from the electrocatalytic oxidation of N_2. Furthermore, no peak corresponding to nitrite appears in the IC curve obtained from electrolyte after NOR test (Figure 2e)-i), evidence of the outstanding selectivity of Pd/PdO-TiO_2@2-MeIm/PPy/GO for electrochemical NOR toward NO_3^- generation.

In order to further investigate the individual contributions of each component in Pd/PdO-TiO_2@2-MeIm/PPy/GO to NOR activity, a group of electrocatalysts is fabricated under consistent conditions, fabricated utilizing distinctive carriers (GO and PPy/GO) or in the absence of a Pd precursor to assess their impact on the activity. The Pd and TiO_2 content of the resulting electrocatalysts are listed in Table S1, determined from inductively coupled plasma-optical emission spectrometry (ICP-OES) results. As illustrated in Figure 2f, neither GO nor PPy/GO exhibits electrocatalytic performance for NOR. In contrast, 2-MeIm/PPy/GO shows limited NOR electroactivity, achieving a NO_3^- yield of 5.2 mg h^{-1} $mg^{-1}_{act.}$ and a corresponding FE of 1.02%. NOR electroactivity in unsupported Pd/PdO-TiO_2 is found to be suboptimal due to pronounced aggregation (Figure S3a), as well as Pd/PdO-TiO2@GO (Figure S3b). Even with the incorporation of PPy/GO, there is only a slight improvement in the aggregation persisted in Pd/PdO-TiO_2 (Figure S3c), while the NOR performance is enhanced with a NO_3^- yield of 13.94 mg h^{-1} $mg^{-1}_{act.}$ and a corresponding FE of 1.80%, possibly caused by the accelerated the electron transport resulting from the good conductivity of PPy. Comparing the SEM images of Pd/PdO-TiO_2@2-MeIm/PPy/GO and Pd/PdO-TiO_2@PPy/GO (Figures 1a and S3c), it is evident that the presence of 2-MeIm facilitates the dispersion of Pd/PdO-TiO_2, resulting in the improved NOR electroactivity of Pd/PdO-TiO_2@2-MeIm/PPy/GO. In addition, the NO_3^- yield and FE of TiO_2@2-MeIm/PPy/GO are significantly lower compared to that of Pd/PdO-TiO_2@2-MeIm/PPy/GO, indicating Pd has a higher nitrogen activation capacity than Ti. The above results well demonstrate that Pd/PdO-TiO_2 serves as the active center for NOR electrocatalysis in Pd/PdO-TiO_2@2-MeIm/PPy/GO and the NOR process mainly occurs on Pd-site.

For further exploring explore the underlying reasons for the sharp decline in the performance of Pd/PdO-TiO_2@2-MeIm/PPy/GO during the sixth cycle, detailed characterizations are conducted on the electrocatalyst after 30 h of electrolysis in N_2-saturated electrolyte. Morphological and crystallographic analyses conducted through SEM, HRTEM, and XRD measurements (Figure S4a–d) demonstrated that there are no discernible alterations in the morphology and crystal structure of Pd/PdO-TiO_2@2-MeIm/PPy/GO, suggesting that no crystalline phase transformations have taken place during the NOR process. However, X-ray photoelectron spectroscopy (XPS) uncovers notable distinctions in the chemical states of the elements present in Pd/PdO-TiO_2@2-MeIm/PPy/GO. Due to the addition of Nafion and the absorption of electrolyte, the additional peaks appear in the XPS spectra of Pd/PdO-TiO_2@2-MeIm/PPy/GO after long term NOR, corresponding to F 1s in the survey spectrum (Figure 3a-ii), CF_2 (291.8 eV),[15] CF_3 (293.5 eV),[16] K^+ $2p_{3/2}$ (292.6 eV),[17] K^+ $2p_{1/2}$ (295.7 eV)[18] in C 1s spectrum (Figure 3b-ii) and OH^- (530.8 eV)[19] and etheric groups in Nafion (535.4 eV)[20] in O 1s spectrum (Figure 3d-ii), respectively. A comparison of the Ti 2p spectra in Figure 3e reveals no change in Pd/PdO-TiO_2@2-MeIm/PPy/GO following the NOR process. The Ti^{4+} $2p_{3/2}$ and Ti^{4+} $2p_{1/2}$ orbitals of anatase TiO_2[21] give rise to two well-separated peaks at 458.6 and 464.3 eV, respectively. It is suggested that the competed OER is dominant at the Ti-site for generating *O and further accelerating the non-electrochemical step of NOR. A comparison between the Pd 3d spectra of Pd/PdO-TiO_2@2-MeIm/PPy/GO acquired prior to and following the NOR reaction reveals a significant difference, as shown in Figure 3f. After Pd/PdO-TiO_2@2-MeIm/PPy/GO synthesized, two pairs of peaks located at 335.5, 340.7 eV and 337.7, 342.8 eV in Figure 3f-i are associated with Pd^0 $3d_{5/2}$, Pd^0 $3d_{3/2}$[22] and Pd^{2+} $3d_{5/2}$,[23] Pd^{2+} $3d_{3/2}$,[24] respectively, well confirming the existence of metallic Pd and Pd—O bonding in the electrocatalysts. Besides the existence of PdO verified by XRD pattern in Figure 1d, Pd^{2+} can be also doped in TiO_2 to form Pd—O bonding. After long term NOR, the spectral features associated with Pd^{2+} $3d_{5/2}$ and Pd^{2+} $3d_{3/2}$ orbits are obviously enhanced and slightly redshift to 338.1 and 343.3 eV in Figure 3f-ii, which may be caused by the formation of Pd—N bonding.[25] Meanwhile, the peak intensity of metallic Pd decrease, indicating that the metallic Pd can be gradually converted into Pd^{2+} during the NOR process, which is further suggested that the conversions of the inert N_2 to active *NO intermediates mostly take place at Pd-site in Pd/PdO-TiO_2@2-MeIm/PPy/GO. Furthermore, prolonged NOR processes lead to the bonding of Pd with nitrogen, further occupying Pd active sites, resulting in a decline in catalytic performance.

3. Conclusion

In conclusion, Pd/PdO-TiO_2@2-MeIm/PPy/GO nanosheets were synthesized by a hydrothermal route. The synergistic effect among the components enhances the Pd and Ti loading capacity, which in turn improves the electrocatalytic NOR performance, as evidenced by a maximum NO_3^- yield of 34.14 μg h^{-1} $mg^{-1}_{act.}$ and a corresponding FE of 5.28% at 2.04 V (versus RHE). GO could provide the high specific surface area and PPy possessed the favorable electrical conductivity for accelerating the electron transfer of NOR, while the introduction of 2-MeIm groups on PPy/GO could facilitate the dispersion of Pd/PdO-TiO_2, which Pd/PdO-TiO_2 served as the active center for NOR elec-

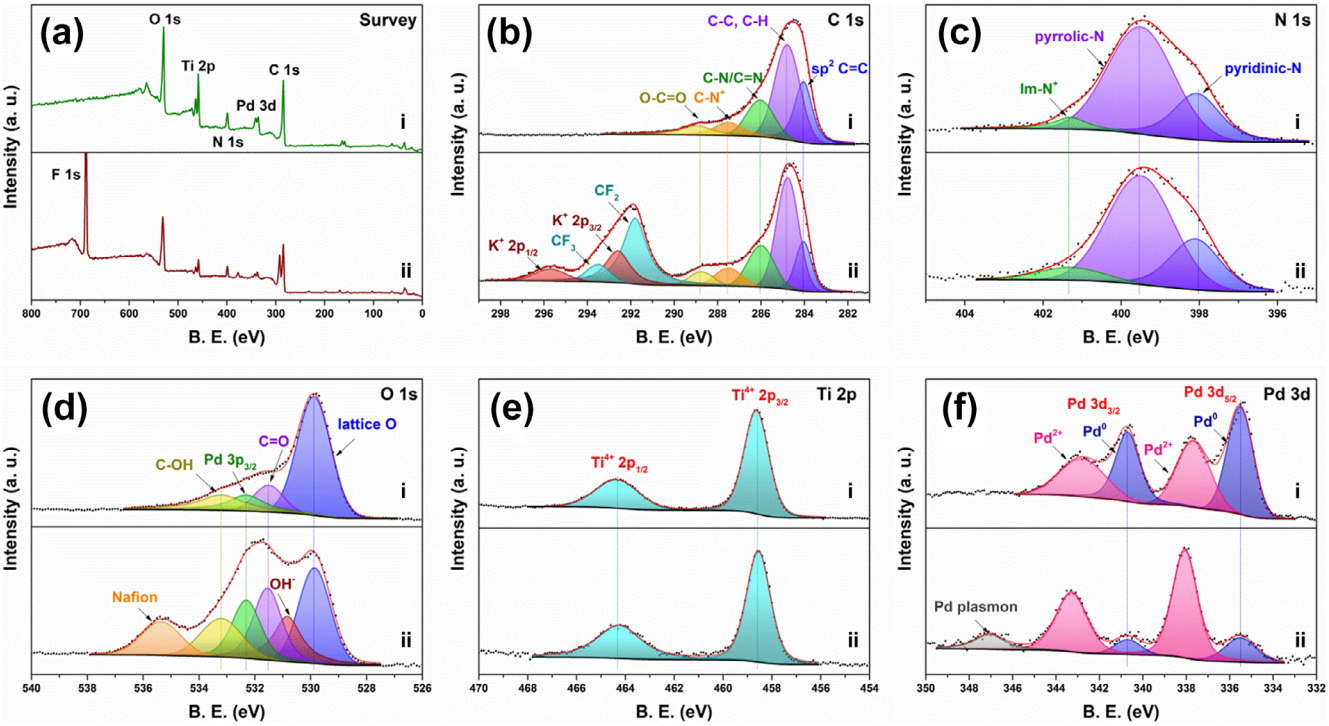

Figure 3. XPS spectra of Pd/PdO-TiO_2@2-MeIm/PPy/GO (i) before and (ii) after electrolysis for 30 h in N_2 saturated electrolyte: a) survey; b) C 1s; c) N 1s; d) O 1s; e) Ti 2p and f) Pd 3d.

trocatalysis in Pd/PdO-TiO_2@2-MeIm/PPy/GO. The NOR process mainly occurred on Pd-site with the conversions of the inert N_2 to active *NO intermediates, and the competing OER, dominant at the Ti-site, generated *O species which subsequently accelerated the non-electrochemical step of NOR. Overall, our study may signify a successful endeavor in the development of high-performance electrocatalysts for the ambient oxidation of N_2.

Acknowledgments

H.M. thanked the Liaoning Revitalization Talents Program (XLYC2007132). R.Z. thanked the Foundation of Liaoning Province Education Administration in 2024 (Independent topic selection - Natural science category - Strategic industrialization project LJ212410163023) and General Program of Natural Science Foundation of Liaoning Province in 2025(2025-MS-295). S.W. thanked the Scientific Research Fund of Liaoning Provincial Education Department (JYTMS20230767). The authors would like to thank Yao Fan and Gao Jilong from Shiyanjia Lab (www.shiyanjia.com) for the ICP-OES and XPS analysis.

Conflict of Interests

The authors declare no conflicts of interest.

Data Availability Statement

The data that support the findings of this study are available from the corresponding author upon reasonable request.

Keywords: 2-methylimidazolium functionalized polypyrrole/graphene oxide (2-MeIm/PPy/GO) · Nitrogen oxidation reaction (NOR) · Pd/PdO · TiO_2

[1] Y. Liu, M. Cheng, Z. He, B. Gu, C. Xiao, T. Zhou, Z. Guo, J. Liu, H. He, B. Ye, *Angew. Chem., Int. Ed.* **2019**, *58*, 731–735, https://doi.org/10.1002/anie.201808177.
[2] J. G. Chen, R. M. Crooks, L. C. Seefeldt, K. L. Bren, R. M. Bullock, M. Y. Darensbourg, P. L. Holland, B. Hoffman, M. J. Janik, A. K. Jones, *Science* **2018**, *360*, eaar6611, https://doi.org/10.1126/science.aar6611.
[3] W. Tong, B. Huang, P. Wang, L. Li, Q. Shao, X. Huang, *Angew. Chem.* **2020**, *132*, 2671–2675, https://doi.org/10.1002/ange.201913122.
[4] D. Wang, N. He, L. Xiao, F. Dong, W. Chen, Y. Zhou, C. Chen, S. Wang, *Angew. Chem., Int. Ed.* **2021**, *60*, 24605–24611, https://doi.org/10.1002/anie.202109905.
[5] H. Mao, Y. Sun, H. Li, S. Wu, D. Liu, H. Li, S. Li, T. Ma, *Adv. Mater.* **2024**, *36*, 2313155, https://doi.org/10.1002/adma.202313155.
[6] H. Mao, H. Li, Y. Sun, S. Wu, Q. Wu, D. Liu, T. Ma, *Chem. Eng. J.* **2024**, *489*, 151414, https://doi.org/10.1016/j.cej.2024.151414.
[7] F. Liu, J. Zhou, M. Sun, Z. Xu, H. Wang, N. Yao, Y. Wang, F. Hao, Y. Xiong, J. Wang, *Angew. Chem.* **2025**, *137*, e202504641.
[8] Y. Ma, L. Guo, L. Chang, W. Guo, T. Zhou, F. Hao, W. Su, J. Zhou, G. Wang, M. Shao, *Nat. Commun.* **2025**, *16*, 7632, https://doi.org/10.1038/s41467-025-63013-0.
[9] Y. Wang, F. Hao, H. Xu, M. Sun, X. Wang, Y. Xiong, J. Zhou, F. Liu, Y. Hu, Y. Ma, *Angew. Chem., Int. Ed.* **2025**, *64*, e202508617.
[10] Y. Xiong, Y. Wang, M. Sun, J. Chen, J. Zhou, F. Hao, F. Liu, P. Lu, X. Meng, L. Guo, *Adv. Mater.* **2024**, *36*, 2407889, https://doi.org/10.1002/adma.202407889.

[11] J. Zhou, F. Liu, Z. Xu, J.-A. Yin, L. Guo, F. Hao, Y. Wang, Y. Xiong, X. Zhou, C. Wang, *J. Am. Chem. Soc.* **2025**, *147*, 23226–23238.
[12] M. Kuang, Y. Wang, W. Fang, H. Tan, M. Chen, J. Yao, C. Liu, J. Xu, K. Zhou, Q. Yan, *Adv. Mater.* **2020**, *32*, 2002189, https://doi.org/10.1002/adma.202002189.
[13] T. Li, S. Han, C. Cheng, Y. Wang, X. Du, Y. Yu, B. Zhang, *Angew. Chem.* **2022**, *134*, e202204541.
[14] T. Li, S. Han, C. Wang, Y. Huang, Y. Wang, Y. Yu, B. Zhang, *ACS Catal.* **2021**, *11*, 14032-14037, https://doi.org/10.1021/acscatal.1c04360.
[15] T. Li, S. Han, Y. Wang, J. Zhou, B. Zhang, Y. Yu, *Angew. Chem., Int. Ed.* **2023**, *62*, e202217411.
[16] Y. Guo, S. Zhang, R. Zhang, D. Wang, D. Zhu, X. Wang, D. Xiao, N. Li, Y. Zhao, Z. Huang, *ACS Nano* **2021**, *16*, 655–663, https://doi.org/10.1021/acsnano.1c08109.
[17] L. Zhang, M. Cong, X. Ding, Y. Jin, F. Xu, Y. Wang, L. Chen, L. Zhang, *Angew. Chem.* **2020**, *132*, 10980–10985, https://doi.org/10.1002/ange.202003518.
[18] Z. Nie, L. Zhang, X. Ding, M. Cong, F. Xu, L. Ma, M. Guo, M. Li, L. Zhang, *Adv. Mater.* **2022**, *34*, 2108180, https://doi.org/10.1002/adma.202108180.
[19] C. Dai, Y. Sun, G. Chen, A. C. Fisher, Z. J. Xu, *Angew. Chem., Int. Ed.* **2020**, *59*, 9418–9422, https://doi.org/10.1002/anie.202002923.
[20] H. Mao, Y. Sun, H. Li, S. Li, D. Liu, Y. Sun, S. Wu, H. Li, T. Ma, R. Zhang, *Electrochim. Acta* **2024**, *482*, 143978, https://doi.org/10.1016/j.electacta.2024.143978.
[21] C. E. Hamilton, J. R. Lomeda, Z. Sun, J. M. Tour, A. R. Barron, *Nano Res.* **2010**, *3*, 138–145, https://doi.org/10.1007/s12274-010-1007-3.
[22] Y. Cai, J. Li, L. Yi, X. Yan, J. Li, *Appl. Surf. Sci.* **2018**, *450*, 102–111, https://doi.org/10.1016/j.apsusc.2018.04.186.
[23] G. Yu, J. Wang, H. Ma, X. Liu, S. Qin, Z. Yang, G. Zhang, Y. Li, L. Zhu, *Chem. Eng. J.* **2021**, *417*, 128111, https://doi.org/10.1016/j.cej.2020.128111.
[24] H. Che, J. Wang, X. Gao, J. Chen, P. Wang, B. Liu, Y. Ao, *J. Colloid Interface Sci.* **2022**, *627*, 739–748, https://doi.org/10.1016/j.jcis.2022.07.080.
[25] S. Wang, T. Wang, X. Wang, Q. Deng, J. Yang, Y. Mao, G. Wang, *Int. J. Hydrogen Energy* **2020**, *45*, 12629–12640, https://doi.org/10.1016/j.ijhydene.2020.02.212.

Manuscript received: July 26, 2025